Mon. Not. R. Astron. Soc. **000**, 1–8 (2015) Printed 19 September 2014 (MN LATEX style file v2.2)

A new prescription for the random magnetic field of the Milky Way

M. C. Beck[1⋆], A. M. Beck[2,3,4]†, R. Beck[5], K. Dolag[2,4], A. W. Strong[3] and P. Nielaba[1]
[1]*Department of Physics, University of Konstanz, Universitätsstr. 10, D-78457 Konstanz, Germany*
[2]*University Observatory Munich, Scheinerstr. 1, D-81679 Munich, Germany*
[3]*Max Planck Institute for Extraterrestrial Physics, Giessenbachstr. 1, D-85748 Garching, Germany*
[4]*Max Planck Institute for Astrophysics, Karl-Schwarzschild-Str. 1, D-85741 Garching, Germany*
[5]*Max Planck Institute for Radioastronomy, Auf dem Hügel 69, D-53121 Bonn, Germany*

Accepted XXXXX. Received XXXXX; in original form XXXXX

ABSTRACT

We present a new prescription for the small-scale magnetic field of the Milky Way and complement existing models for the total Galactic magnetic field. In particular, we extend the random and striated magnetic field components of the Jansson & Farrar (JF12) model and investigate the characteristics of random magnetic fluctuations. Thereby the small-scale magnetic field is modelled by Gaussian random fields using a random magnetic field power spectrum. We update the spatial distribution of Galactic cosmic ray electron density by a recent GALPROP model.

We derive full-sky projections of the total and polarized synchrotron intensity as well as the Faraday rotation measure distribution of our model and compare to real data. We obtain good agreement to the WMAP7 22 GHz polarized and total intensity emission maps and we retrieve improved fits to Galactic foreground rotation measure maps and power spectra of Oppermann et al. Our new prescription significantly complements previous models of the GMF and reveals implications for future studies on the deflection of ultra high energy cosmic rays (UHECR).

Key words: cosmic rays – Galaxy: general – ISM: magnetic fields – magnetic fields

1 INTRODUCTION

Magnetic fields are an important property of every astrophysical system and also of the Milky Way. Over the past years we gained more and more insight into the magnetic field of our Galaxy and its structure on large and on small scales. From radio observations (see e.g. Beck et al. 1996) we can constrain the Galactic magnetic field (GMF) and the physical processes responsible for its creation. Within galaxies in general, and thus also within our Milky Way, magnetic fields are commonly generated by dynamo action. These dynamos operate on very small seed fields, which might already have been present even before the first galaxies appeared in the Universe (for reviews on cosmic magnetism see e.g. Beck & Wielebinski 2013; Widrow 2002). The detailed structure of the GMF is still under debate, however, recent observational advancements significantly improve our knowledge on large-scale and small-scale features of the GMF (e.g. with the PLANCK mission Planck Collaboration 2014a,b,c,d,e). From the extensive literature about the GMF we want to point out the well-written reviews from Haverkorn (2014); Noutsos (2012); Heiles & Haverkorn (2012). The total GMF is usually split-up into several small-scale and large-scale fields. However, in the literature different and thus confusing notations are used for these components: the large-scale field is often called regular, uniform or coherent (see e.g. Jaffe et al. 2010) and the small-scale fields are referred to as random, tangled or turbulent fields. Most recently, another type of field has been considered to complement the small-scale field: often referred to as anisotropic random (see e.g. Orlando & Strong 2013), ordered random (see e.g. Jaffe et al. 2010) or striated field (see e.g. Jansson & Farrar 2012a). The striated field is characterized by having one main axis where the direction can fluctuate and it has a mean value of zero. Possible candidates for the origin of such fields are compression or shear of magnetized turbulent gas e.g. by supernova shocks or density waves in spiral arms (see e.g. Haverkorn 2014). The clearest indication of anisotropic random fields are given by radio observations of M51 (Fletcher et al. 2011). The various components of the total magnetic field can be distinguished by their different contributions to observables such as total synchrotron intensity (I), polarized intensity (PI) and rotation measure (RM) (see e.g. Beck & Wielebinski 2013).

Until recently, most studies focused on modelling the large-scale GMF. However, lately, the small-scale field component is gaining attention: Miville-Deschênes et al. (2008) use 408 MHz total synchrotron data and 22 GHz WMAP polarized synchrotron data to determine a bisymmetric spiral structure (BSS) of the large-scale halo field and a random component with about half the am-

⋆ E-mail: marcus.beck@uni-konstanz.de
† E-mail: abeck@usm.lmu.de

plitude of the regular component. Jaffe et al. (2010) consider 408 MHz I data, WMAP 22 GHz PI data and 269 extragalactic RM sources and found an axisymmetric spiral structure (ASS) of the large-scale disk field model and random and anisotropic small-scale field strengths five respectively four times as large as the regular component. Fauvet et al. (2011, 2012) consider WMAP 5 I 22 GHz, ARCHEOPS 353 GHz and 408 MHz I data and found a modified logarithmic spiral structure and a random small-scale amplitude which is a fourth as large as the large scale amplitude. Sun et al. (2008) determine random fields with a strength of about 3 μG to give the best fit to the ASS model for the disk and find an odd symmetry in the halo. In Sun & Reich (2009) the before mentioned model is used to simulate 1.4 GHz synchrotron emissions at arcsec angular resolution. Thereby I, PI and RM of selected patches of the sky are studied. The random magnetic field component therein is modelled to follow a Kolmogorov type random field and no anisotropic random field is considered. Most recently, models with different magnetic field configurations for the disk as well as for the halo are developed. Jansson & Farrar (2012a) combine significantly different models for the Galactic disk and halo. The successful application of their model suggests that disk and halo field structures cannot be modelled by scaled-up versions of the same magnetic field configuration. Their best-fit model has even symmetry in the disk and odd symmetry in the halo. We base our modifications and advancements on their already very sophisticated model for the GMF.

We use the HAMMURABI code (Waelkens et al. 2009) to compute full-sky mock observations of various models of the Galactic magnetic field, the cosmic-ray (CR) electron density $n_{\rm CRe}$ and the thermal electron density $n_{\rm e}$. Calculated mock observations are Galactic rotation measure (RM), synchrotron maps of total intensity (I), Stokes parameters Q and U (and therefore polarized synchrotron intensity (PI) and polarization angle (PA)) and deflection maps for ultra high energy cosmic rays (UHECR). For the thermal electron density we use the widely accepted NE2001 model (Cordes & Lazio 2002). The most prominent large-scale features of the model are spiral arms and a molecular ring component. There are only few small-scale features embedded: A galactic center component as well as local ISM structures and underdense regions. There are no spatial fluctuations modelled by an energy spectrum of the thermal electron density n_e in the NE2001 model and this model is quite smooth elsewhere.

The model for $n_{\rm CRe}$ used here, is identified by its GALPROP ID 54_z04LMPDS and is described in detail in Strong et al. (2010). It was produced with the GALPROP software; for a full account of the method see Strong, Moskalenko, & Ptuskin (2007)[1]. Models using the same electron distribution are extensively compared with synchrotron data in Orlando & Strong (2013). Briefly, this model uses a radial Galactic distribution of cosmic-ray electron sources based on the distribution of pulsars, since these are a tracer of supernova remnants, which are thought to be the sources of CR. The radial distribution is extended to $R = 15$ kpc to account for gamma-ray and synchrotron observations of the outer Galaxy as described in Orlando & Strong (2013). The propagation region has a vertical height of 4 kpc from the Galactic plane and a radius of 20 kpc. Cosmic-ray propagation is by pure diffusion without reacceleration, since this is found to give better agreement with synchrotron radiation from the Galaxy (Strong, Orlando, & Jaffe 2011). The electron spectrum in this model is consistent with the measurement at the solar position with Fermi-LAT, in the range 10 GeV to 1 TeV (see the illustration in Fig. 1). We find a difference of factor 1.4 between the $n_{\rm CRe}$ data used by JF12 and our data.

[1] see http://galprop.stanford.edu; latest versions available at http://sourceforge.net/projects/galprop

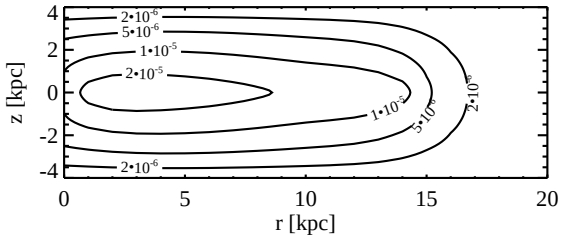

Figure 1. Spatial distribution of relativistic electrons in the Milky Way calculated from particle spectra derived from the GALPROP model with ID 54_z04LMPDS. The contour levels represent the density of electrons in terms of the coefficient C in $N(\gamma)d\gamma = C(r)\gamma^{-p}$, units cm^{-3} (see Appendix A).

In addition to the recent progress in modelling the GMF, numerical simulations of galaxies start to contribute to our understanding on the seeding of magnetic fields in collapsed cosmic structures (see e.g. Beck et al. 2012, 2013) and will hopefully soon provide us with reasonable simulated models of magnetic fields in galaxies.

RM observations are a useful tool to study the magnetic field in our Galaxy and its halo (see e.g. Pshirkov et al. 2011; Mao et al. 2010, 2012). In particular, small-scale fluctuations within the RM data (see e.g. Schnitzeler 2010; Oppermann et al. 2012, 2014) can be used to study the random and turbulent components of the GMF. Based on these observational results we want to investigate the small-scale magnetic fields. The model of Jansson & Farrar (2012a,b) is not yet able to reproduce fluctuations in the full-sky maps. In this work, we overcome this problem and present an improved prescription for the small-scale magnetic field of the Milky Way.

The paper is organized as follows. We show our modifications to the JF12 model in Section 2. In Section 3 we present our improved galactic observables and investigate implications for UHECR propagation. We summarize and conclude in Section 4.

2 MODIFYING THE JF12 RANDOM FIELD MODEL

We base our investigations on the large-scale model of Jansson & Farrar (2012a) for the Galactic magnetic field. Their model contains separate components for the magnetic field patterns within the spiral disk, the toroidal halo field and the X-shaped poloidal halo field. Each of these components are modelled in a way to ensure zero magnetic divergence. In addition to the large-scale field components an anisotropic random field is introduced ('striated' random field). This striated random field is totally aligned to all components of the large-scale field (i.e. spiral disk and both halo field components). Furthermore, Jansson & Farrar (2012b) complement the model with a purely isotropic random field. This model is independent of the large-scale model and its spiral disk strengths and halo components are individually determined. The detailed method for obtaining both the parameters and the quality of the fits of the models are given in Jansson et al. (2009).

We label the original field components from our base mod-

els with the index 'JF12' and make use of the following variable names: $B_{\rm reg}$ represents the large-scale field and $B_{\rm aniso}$ and $B_{\rm iso}$ represent the (an)isotropic small-scale fields. The corresponding small-scale models in JF12 are: $B_{\rm striated,JF12}$ and $B_{\rm rand,JF12}$. Unchanged field components in our modifications are still denoted as JF12.

In the JF12 model for the polarized intensity only the regular and the striated field have to be taken into account. Therefore, the following simple addition is performed, because the striated field is aligned with the large-scale regular field with an amplitude of $B^2_{\rm striated} = \beta \cdot B^2_{\rm reg,JF12}$ and the PI is computed by replacing

$$B^2_{\rm reg,\perp} \rightarrow \alpha(1+\beta) B^2_{\rm reg,JF12} \sin^2\theta. \quad (1)$$

Thereby, θ is the angle between the integration line-of-sight (LOS) and the vector of the large-scale magnetic field such that $B^2 \sin^2\theta = B^2_\perp$. We use the original parameters $\gamma = \alpha(1+\beta) = 2.92$ and $\beta = 1.36$ from the JF12 model. β describes the strength of the striated field component. α is a scaling factor for the cosmic-ray electron density $n_{\rm CRe}$, because in the optimisation process the strength of the small-scale magnetic field and the rescaling of $n_{\rm CRe}$ are degenerate. Due to the difference in the new GALPROP data set $n_{\rm CRe}$ is upscaled by a factor of 1.4. This would correspond to using $\alpha = 1.73$.

The influence on the total synchrotron intensity by the (an)isotropic random magnetic field is accounted for by replacing $B^2_{\rm reg}$ with

$$B^2_{\rm reg,\perp} \rightarrow \alpha(1+\beta) B^2_{\rm reg,JF12} \sin^2\theta + \frac{2}{3}\alpha B^2_{\rm rand,JF12}. \quad (2)$$

In the JF12 model one sufficiently large volume element of the perpendicular component of the random magnetic field averages to $\langle B^2_{\rm rand,\perp}\rangle = 2/3 \cdot B^2_{\rm rand}$, which is accounted for by the second term of Eq. (2) and is independent of the angle θ. $B_{\rm rand,JF12}$ in this model is a scalar amplitude giving a large-scale distribution of the strength of the isotropic random field.

The different components of the small-scale magnetic field contribute differently to each of the observables (e.g. the striated random field contributes to I and PI, and the random field only contributes to I). It is assumed that the fluctuations have such small scales so that they average out in the corresponding observational integrals. Therefore, there is no influence of the small-scale model to RM or UHECR deflection maps in the JF12 model.

The two above introduced assumptions for replacing $B^2_{\rm reg}$ in the original formulation of the JF12 model only hold if the number of volume cells with small-scale fluctuations along the LOS ℓ is large to allow for the fluctuations to average out. For example, in the observational integral along the LOS for the RM ($\sim \int_\ell n_e (B_\parallel + b_\parallel) dl$) the term $b_\parallel$ for the small-scale magnetic field is not negligible and does not average out. Since we want to allow for larger fluctuations, the assumptions of the JF12 model do not hold and we improve their previous description of the total magnetic field by introducing individually computed realizations of the small-scale field

$$\boldsymbol{B}_{\rm tot} = \boldsymbol{B}_{\rm reg,JF12} + f_a \boldsymbol{B}_{\rm aniso} + f_i \boldsymbol{B}_{\rm iso}. \quad (3)$$

This modification holds for all observables and no additional assumptions on the influence on different observables are necessary besides the usual LOS integrations. The parameters f_i and f_a are introduced to allow for a rescaling of the JF12 random field strengths. The contributions of the (an)isotropic field components are now vector quantities with a functional form as follows. The isotropic random field is realized by

$$\boldsymbol{B}_{\rm iso} = B_{\rm rand,JF12} \cdot \boldsymbol{\mathcal{G}} \quad (4)$$

where $B_{\rm rand,JF12}$ gives a scalar amplitude of a large-scale distribution of the isotropic random field. It consists of a spiral disk and a halo component. $\boldsymbol{\mathcal{G}}$ is a three dimensional divergence-free Gaussian random field with $\langle \boldsymbol{\mathcal{G}} \rangle = \boldsymbol{0}$ and $\langle |\boldsymbol{G}|^2 \rangle = 1$ following an arbitrary power distribution of k in Fourier-space. We use a modified version of the GARFIELDS code (Kitaura & Enßlin 2008) for the vector computation of the Gaussian random fields. We generate a stochastic realization of such a Gaussian random field with a power spectrum $P(\boldsymbol{k})$ with the help of an inverse Fourier transformation (see e.g. Martel 2005), in principle written as

$$B(\boldsymbol{x}) \propto \int \sqrt{P(\boldsymbol{k})} (\chi - i\zeta) e^{(i\boldsymbol{k}\cdot\boldsymbol{x})} d\boldsymbol{k}, \quad (5)$$

where χ and ζ are random numbers drawn from a Gaussian random distribution. Here $k = 2\pi/l$ is the wave vector and l the spatial scale. The anisotropic random field is modelled by

$$\boldsymbol{B}_{\rm aniso} = \sqrt{\frac{3}{2}}\beta \cdot \frac{\boldsymbol{\mathcal{G}} \cdot \boldsymbol{B}_{\rm reg,JF12}}{|B_{\rm reg,JF12}|^2} \boldsymbol{B}_{\rm reg,JF12}. \quad (6)$$

This formulation ensures that the resulting magnetic field vector has an orientation which is aligned along the large-scale field vector of the JF12 model $\boldsymbol{B}_{\rm reg,JF12}$ and is parallel or anti-parallel to the large-scale field. The pre-factor $\sqrt{3/2}$ compensates the reduction of $\boldsymbol{\mathcal{G}}$ by one dimension due to the projection. Sign and strength both vary on small scales. This formulation gives the striated field as the description in JF12 suggests. Therefore the anisotropic random field follows the large-scale field structure and has a spiral disk and poloidal and toroidal halo components.

We assume the power distribution of the Gaussian random field $\boldsymbol{\mathcal{G}}$ to be of Kolmogorov type. The lower limit for k is given by $k_{\rm min} = 2\pi/L_{\rm max}$ and the upper limit of k is determined by the spatial resolution at the Nyquist limit $k_{\rm max} = 2\pi/L \cdot N/2$, where L is the box size and N the number of grid cells in such a box. We compute both random components from a three dimensional realization of a spectral power distribution. The spatial resolution throughout the whole sampled volume is 20 pc.

3 RESULTS

In this section we present the results of our new model for the GMF. We use the HEALPix pixelisation scheme by Górski et al. (2005), with a resolution parameter of NSIDE $= 128$. Therefore, the angular resolution of the final maps is approximately 27 arcsec. At first, the HEALPix-map pixel is sampled along the LOS into a '3D-HEALPix grid' as suggested by Jaffe et al. (2010). This results in a conical shape of the volume cells along this line, i.e. the volume units increase with distance l along the LOS. The resolution is enhanced by splitting one such beam into 4 sub-beams and is performed repeatedly in such a way that the spatial resolution is kept similar to the resolution of the random field grid and also accounts for sub-beam depolarization. We simultaneously compare all computed observables to the observation data. Furthermore, we follow Oppermann et al. (2012) in our analysis of the RM data, which we take from the updated full-sky map of Oppermann et al. (2014) and we denote the observational data as O12.

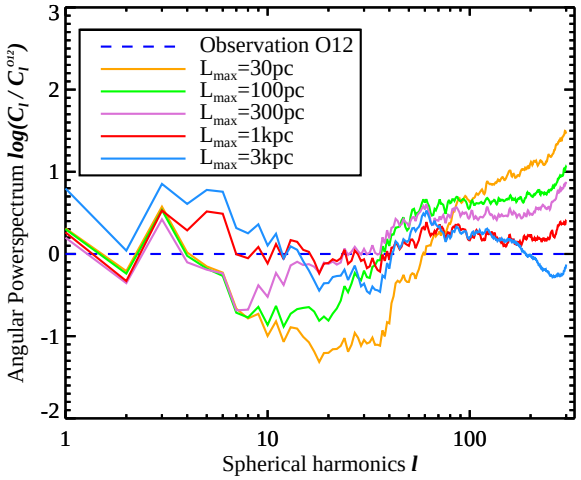

Figure 2. Comparison of simulated RM signal map power spectra (solid lines) for various length scales of the turbulent magnetic field power spectrum. We normalise all the power spectra to values derived from the O12 data (dashed line and Fig. 4). We find the best fit at a maximum length scale of 1 kpc.

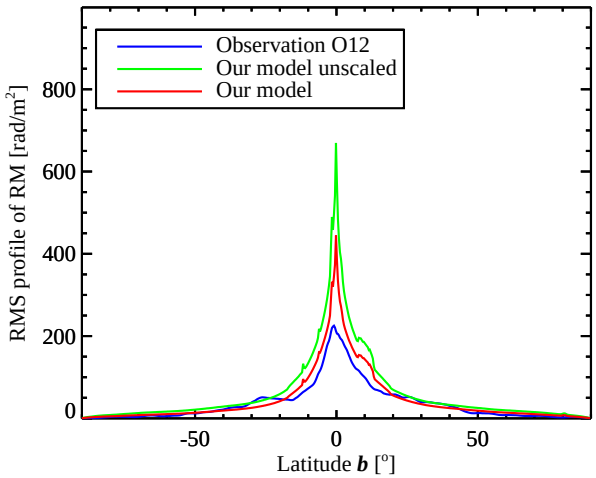

Figure 3. RMS profiles of RM distributions as a function of Galactic latitude. We show a profile derived from the Oppermann et al. (2012) RM data (blue line) as well as profiles corresponding to our new prescription with different scaling values for f_i. The green line corresponds to the JF12 parameter values ($f_i = f_a = 1$) and the red line corresponds to our best fit values.

3.1 Synchrotron and RM full-sky maps

At first, we adapt the amplitudes of the two small-scale magnetic field components of the JF12 model. The new prescription of the small-scale magnetic field leads to contributions of the small-scale fluctuations to the full sky maps, which are not present in the JF12 model. They appear, because larger scales are allowed and do not average out as assumed in JF12, where too few large-scale fluctuations along the LOS are present. This is illustrated in Fig. 2, which shows the larger the maximum length scale of the random field $L_{\rm max}$ is, the more power is present in the full sky map at larger angular scales (smaller l). We find a value of $L_{\rm max} = 1$ kpc (red line) to fit best to the observational data (horizontal line).

We follow Oppermann et al. (2012) and compute the root mean square (RMS) profiles of the RM maps as a function of Galactic latitude b. As we show in Fig. 3 an unscaled small-scale magnetic field leads to a dominant contribution of the random magnetic field and large-scale features of the RM map vanish (not shown). We set f_i to 0.6 and f_a to 0.3 and rescale the amplitude of the random magnetic field and obtain the best-fit to the observational maps and a RMS profile curve, which also fits best to the observational data.

Fig. 4 shows that after rescaling the amplitude of the random field the shape and quality of the angular power spectrum is still preserved. Since the observational map results from one realization of infinitely many possible ones, we compare the spectrum of the observational map to a sample of 100 realizations. We show the mean values as well as confidence levels of $1-3$ standard deviations σ.

Fig. 5 shows a full-sky comparison of mock observations of our model, the JF12 model and observational data. We compare the total synchrotron intensity, the polarized synchrotron intensity, the polarization angle as well as the rotation measure distribution. Our model compares very well with the observational data for the large-scale features of the map and is also in good agreement with the observational data for the small-scale features. Most importantly,

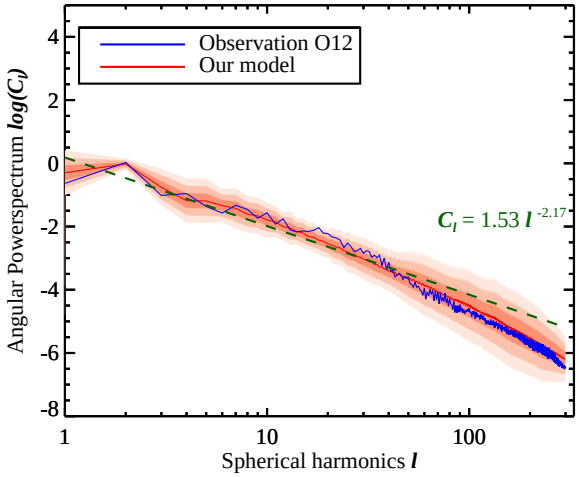

Figure 4. We show the power spectrum of the signal map corresponding to the Oppermann et al. (2014) RM map (blue line). Additionally, we plot the mean power spectrum of the signal map derived from our new model (red line), where the contour levels represent a standard deviations of 1σ, 2σ and 3σ. We derived the mean and standard deviations from a sample of 100 simulated realizations of the turbulent magnetic field power spectrum.

the JF12 model is unable to reproduce small-scale structures in the full-sky maps.

We discuss the contribution of the different magnetic field components to the observables. The Haslam 408 MHz data (Haslam et al. (1981) and Haslam et al. (1982)) gives good access to foreground synchrotron emission. In this unpolarized data all components of the magnetic field contribute to the synchrotron emissivity: large-scale field components and both small-scale com-

ponents, i.e. anisotropic and isotropic random field. We find good agreement with the overall large-scale structure of the map for our model. We notice that the map of the JF12 model with the synchrotron contribution as described in Sec. 2 does not give any small-scale features in the synchrotron maps (due to the smooth distribution of the cosmic ray electrons). We note that the overall amplitude of the total intensity in the map of the JF12 model gives slightly too high emission. Furthermore, we compare to the polarized synchrotron map of the WMAP 7 22 GHz data. In the JF12 model only the large-scale and striated magnetic field components contribute to the polarized intensity, but in our model this map gives access to all the magnetic field components as already mentioned. In our model we find good agreement with the large-scale structure as well as small-scale features which are not replicated by the JF12 model. Additionally, we find a similiar good agreement of the polarization angle.

At last, we compare to the RM map of Oppermann et al. (2014). In the JF12 model the RM is unaffected by small-scale magnetic field structures, because they are assumed to average out completely along the entire LOS. We note that the map of the JF12 model does only give some localised small-scale features in the RM map which result from the implementation of local features in the NE2001 model for the thermal electrons, but not from the magnetic field model itself. Again, we find good agreement of our model with the large-scale structure as well as with the small-scale structures, which is substantiated by the spectrum analysis on this map (see before).

In order to investigate the vertical magnetic field towards the Galactic poles the RM data at Galactic latitudes $|b| \geqslant 77^\circ$ are compared to Mao et al. (2010). More than 1000 polarized extragalactic radio sources reveal a median RM values of 0.0 ± 0.5 rad/m^2 for the north pole respectively 6.3 ± 0.7 rad/m^2 towards the south Galactic pole. We find median values of -3.2 ± 2.5 rad/m^2 respectively 4.7 ± 2.9 rad/m^2 for 2520 HEALPix pixels in each direction. We claim that one realization of our model among the many possible one can be found which fits to the observed data. Moreover with our model it can be inferred that the RM values for the north and south Gaactic pole are dominated by the random field and its realization and is not necessarily restricted to the large scale magnetic field.

We note that the size of structures in the maps differs throughout the entire maps. We exemplary discuss this for the RM map: We see larger structures for high values of absolute latitude and small structures in the disk part. We conclude that this is due to the contribution of the thermal electron density n_e along the LOS. The LOS, which permeate the Galactic halo n_e are shorter than the LOS permeating disk structures. Because n_e modulates the contribution of the magnetic field to RM this leads to near structures appearing larger in the map, because of their higher angular extent. In the disk the angular extent is smaller, because of the contribution of structures that are further away (see also similar findings by Sun & Reich 2009).

3.2 UHECR deflection

Fig. 6 shows the deflection map of UHECR protons with energy of 60 EeV. The overall shape of the deflection map is well preserved, but we find small-scale structures as well as in general slightly larger values of deflection angles.

Fig. 7 shows the fraction of the sky over which UHECR deflections (for 60 EeV protons) are larger than a threshold deflection angle of δ_{th}. We find that deflections larger than 10° only

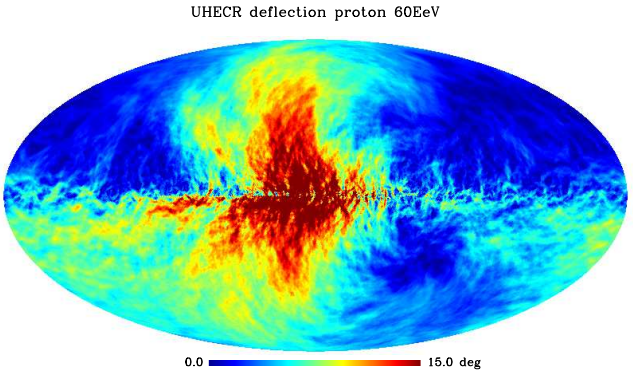

Figure 6. Galactic deflection map for a 60 EeV proton. We show the absolute magnitude of the deflection, displayed by arrival direction. In our new prescription for the GMF we are able to resolve the small-scale features in the deflection characteristics of UHECR.

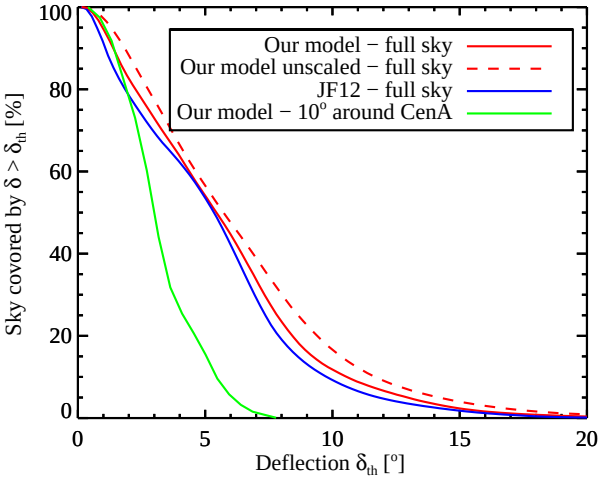

Figure 7. Cumulative fraction of the sky with deflection angle larger than threshold deflection δ_{th}. We show the deflections for our model, the original JF12 GMF model and the deflection of an area of 10 degree around the direction on the sky pointing to CenA. The shown curves are for UHECR with energy of 60 EeV.

cover approximately ten per cent of the sky. It can be seen that our model yields slightly higher values of deflection angles than the JF12 model. The large-scale distribution is conserved, but we find large changes in the local distribution of the deflection angles. Such local structures are not resolved by the JF12 model, because of the insufficient treatment of the small-scale magnetic field therein. We conclude that with our model predictions on the source of UHECRs are possible with significantly improved accuracy.

We find that the small-scale structure of the UHECR deflection maps vary for different realizations. In order to estimate the influence of choice of realization of the small-scale magnetic field on the UHECR deflection maps, we calculate the standard deviation of each pixel of the deflection map by varying the small-scale random field realizations. Fig. 8 shows that the deflection in the central part of the Galactic disk is stronger affected by the choice of the random field realization.

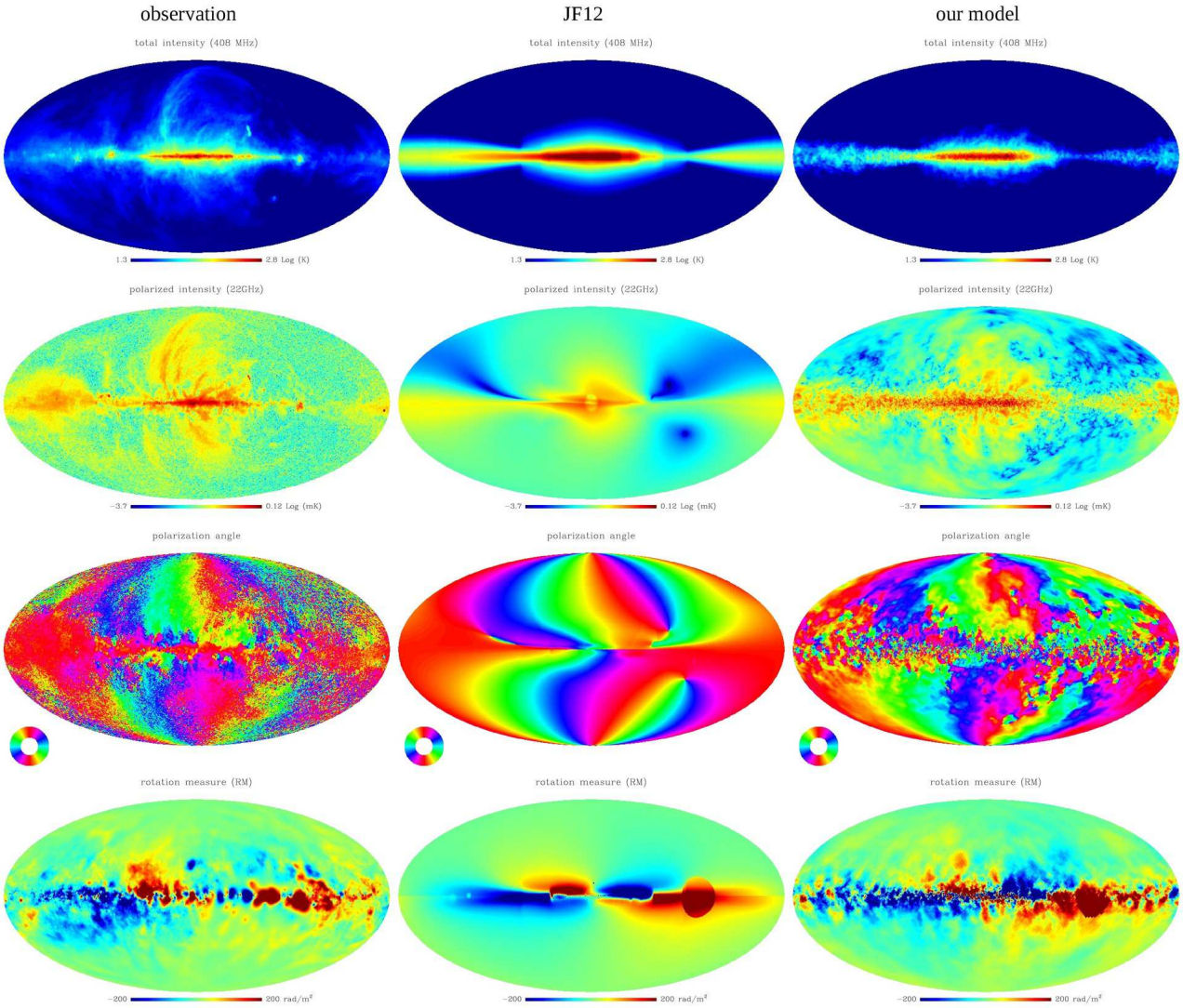

Figure 5. Mollweide projections of observations and simulated data. In each of the maps, the Galactic longitude is zero in the centre and increases to the left. We show (from top to bottom) the total synchrotron intensity, the polarized synchrotron intensity, the polarization angle and the rotation measure distribution. We show (from left to right) the observed quantities, the JF12 model predictions and our new model predictions. For the comparison we use the total 408 MHz intensity data of Haslam et al. (1981) and Haslam et al. (1982), the polarized intensity and polarization angle as given by WMAP 22 GHz observations and the RM map of Oppermann et al. (2014). In our new model for the GMF we resolve the small-scale features in all of the observed quantities very well.

Farrar et al. (2013) and Farrar (2014) discuss the deflection of UHECRs in the JF12 model and compare to other GMF models. They predict Centaurus A (Cen A) as the most possible candidate for the origin of UHECRs. Cen A is the closest active galactic nucleus and is known as a bright radio source (see Fig. 9). They show the arrival directions of protons assuming different GMF models. The uncertainties of the arrival direction presented in their article originates from uncertainties of the optimized model parameters. The deflection which results from any type of random magnetic field is not included and only large-scale features are considered.

Similarily to Giacinti et al. (2011) we claim that small-scale features must be taken into account for studies of UHECR deflection. Keivani A., Farrar G. R. & Sutherland M. (2015) present simulations of trajectories of UHECRs from Cen A to earth. They use the JF12 model as well as the isotropic random component of the JF12 model $B_{\mathrm{rand,JF12}}(\boldsymbol{r})$, but they neglect the influence of the anisotropic random field. They study the impact of different random realizations and coherence lengths up to $20 - 100$ pc (L_{max} up to 512 kpc), but do not discuss their choice of coherence length. In this article, we are able to bridge the gap and motivate the choice of coherence length.

Fig. 10 shows a zoom-in on the region around Cen A. In Keivani A., Farrar G. R. & Sutherland M. (2015) the source directions of the UHECRs are supposed to lie in the regions of the radio lopes of Cen A (for the huge extent of the lobes see Fig. 9). Therefore, a region of 3 degree around the center of Cen A is chosen as the origin of the calculated UHECR trajectories. The UHECRs are deflected by the large-scale field of JF12 model towards lower longitude and lower latitude (see Fig. 10).

Fig. 10 shows the deflection around CenA and as already illustrated in Fig. 7 the deflection varies with the choice of the realization of the random fields. We calculate a mean value of $\mu \approx 3.7^{\circ}$

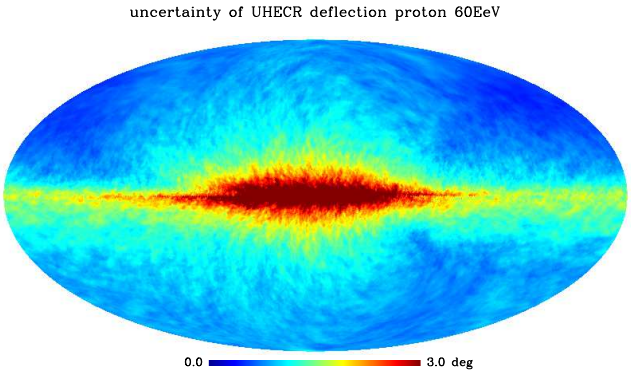

Figure 8. Map of the standard deviation of Galactic deflection maps. The standard deviation was calculated for a number of 100 different small-scale random field realizations. The deflection in the direction towards the center and the disk is more affected by the choice of the realization than the directions towards the Galactic poles.

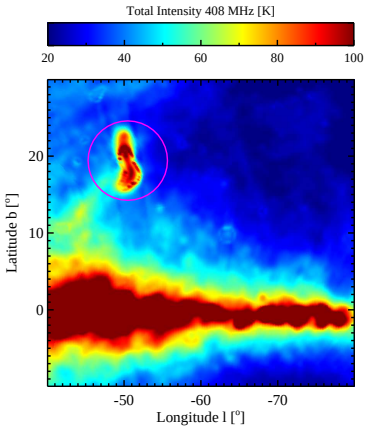

Figure 9. Zoom-in on the Haslam 408 MHz synchrotron intensity map around Cen A (indicated by the purple sign). The huge extend of the radio loops can clearly be seen. Fig. 10 also shows the deflection for the same region of sky.

as well as a standard deviation of $\sigma \approx \pm 1.25^\circ$ for the deflection at a region on the sky of 10° around Cen A.

4 CONCLUSIONS

The statistical properties of the GMF play an important role in solving long-term astrophysical problems such as the propagation of cosmic rays throughout our Galaxy. In this paper, we show that small-scale magnetic field components are not negligible. Electron density fluctuations are commonly assumed to couple to magnetic field fluctuations (due to turbulent motions of the gas) and therefore, predictions of the magnetic field fluctuations from our calculations remain uncertain, because we do not include any fluctuations of electron density. It is important to remember, that the observational maps only give access to multiplied and integrated quantities (e.g. $n_e \cdot B_\parallel$ in the RM). The NE2001 description of thermal electrons does not include spatial fluctuations modelled by an energy spectrum. Thus, the obtained spectrum of the magnetic field could

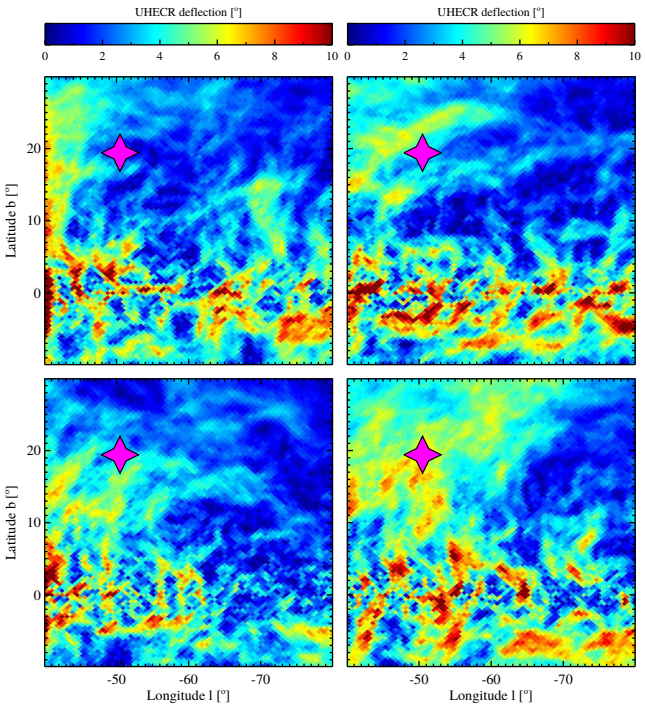

Figure 10. Zoom-in on the Galactic deflection map (see Fig. 6) for a 60 EeV proton around Cen A (indicated by the purple sign). We show the absolute magnitude of the deflection, displayed by arrival direction. The UHECRs originating from Cen A are deflected by the large-scale field of the JF12 model towards lower longitude and lower latitude.

also be part of the fluctuations in n_e. However, the spectrum of the fluctuations of the thermal electrons are expected to follow a Kolmogorov-like power law (Armstrong et al. 1995). Sun & Reich (2009) succesfully apply the NE2001 thermal electron distribution in combination with a Kolmogorov power spectrum for the turbulent magnetic field. We confirm their approach and discuss why such choice is reasonable.

The GMF is usually described as the sum of several large-scale and small-scale components. Candidates for causes of such small-scale features in the magnetic field are interstellar turbulence, supernova explosions and remnants, which induce small-scale distortions into the large-scale field. Such small-scale fields can interact with shocks and are altered by the dynamics of the gas, magnetic reconnection or a wide range of complex physical processes. Our typical length scale of the small-scale field is of the order of some hundreds of parsec. The correlation length L_c of a Gaussian random field can be defined (see Eq. (2.4) in Harari et al. 2002) as

$$L_c B_{\rm rms}^2 = \int_{-\infty}^{\infty} \langle \boldsymbol{B}(0) \cdot \boldsymbol{B}(\boldsymbol{x}(l)) \rangle \, {\rm d}l, \tag{7}$$

where $\boldsymbol{x}(l)$ is a point in space displaced by distance l. Eq. (2.6) of Harari et al. (2002) gives the following formula for computing the correlation length L_c for a Gaussian random field that is sampled between $k_{min} = 2\pi/L_{max}$ and $k_{max} = 2\pi/L_{min}$ with a power law and slope n

$$L_c = \frac{1}{2} L_{max} \frac{n-1}{n} \frac{1-(L_{min}/L_{max})^n}{1-(L_{min}/L_{max})^{n-1}}. \tag{8}$$

A Kolmogorov spectrum ($n = 5/3$) results in $L_c \approx L_{max}/5$ for broad spectra. Therefore, our best-fitting small-scale field has a correlation length of approximately 220 pc.

Regions of supernova and superbubble explosions are believed to be the main source of energy on scales of about 100 pc. Large loops of radio emission such as the North Polar Spur or Loop I to IV show influence of localised features on magnetic fields and therefore also on the observational maps. Supernovae which are blowing bubbles in the ionized interstellar gas, dragging the magnetic field with the gas are good candidates for injection of turbulence into the GMF on scales of about 100 pc. Such structures exist throughout the entire Galaxy and affect the large-scale structure of the magnetic field. Our resulting large length scales of the (an)isotropic random field do strengthen this argument. Detailed models of magnetic fields are important for studying the sources and propagation of Galactic and extragalactic cosmic rays. Detailed knowledge is also necessary to predict the distributions of arrival directions of cosmic rays of energies above 10^{19} eV. Dolag et al. (2004) investigate deflections of UHECRs in constrained simulations of extragalactic magnetic fields and conclude that astronomy with charged particles is possible.

In the last decade, a new generation of UHECR observatories came into operation: the Pierre Auger observatory in the Southern hemisphere and the Telescope Array in the Northern hemisphere, respectively. In the future it may be possible to acquire the GMF structure from direct observations of arrival directions of UHECR for example with this new generation of cosmic ray observatories (for recent and future outcome see e.g. Letessier-Selvon et al. (2013)). The sources and composition of UHECRs are still too uncertain to constrain any GMF models, yet. Most interestingly, a well constrained prescription of the GMF could be a well suited tool to constrain the arrival directions of UHECRs and determine their sources.

ACKNOWLEDGEMENTS

We thank Glennys Farrar, Niels Oppermann and Ann Mao for useful comments and discussions. AMB, KD and RB are supported by the DFG Research Unit 1254. AMB and KD are supported by the DFG Cluster of Excellence 'Origin and Structure of the Universe'. We acknowledge computing time from John von Neumann-Institute for Computing (NIC), Jülich.

APPENDIX A: CONVERSION OF COSMIC RAY ELECTRON DATA

The cosmic ray electron distribution provided by GALPROP was converted to a form suitable for HAMMURABI as follows. HAMMURABI requires the density in the form $N(\gamma)d\gamma = C(r)\gamma^{-p}$, where $\gamma = E/m_e$ is the electron Lorentz factor, and r is the position in the Galaxy. Although the units are cm^{-3}, this quantity does not represent the actual density of CRe, but is a scaled representation of this. GALPROP provides the flux $I(E)$ at (R, z) in cm^{-2} sr^{-1} s^{-1} MeV^{-1} (the GALPROP FITS file has actually $E^2I(E)$ in MeV^2 cm^{-2} sr^{-1} s^{-1} MeV^{-1}). Using $N(\gamma)d\gamma = N(E)dE$, a power-law E^{-p}, and a factor $4\pi/c$ to convert from flux to density, we arrive at $C(r) = (4\pi/c)m_e(E_o/m_e)^p I(R, z, E_0)$, where E_0 is a reference energy. We use $E_0 = 10$ GeV and $p = 3$, as in HAMMURABI. This is a reasonable approximation above 10 GeV, which is the principal range contributing to the synchrotron emission studied in this paper. The input GALPROP file and HAMMURABI format for our model are available on request.

REFERENCES

Armstrong J. W., Rickett B. J., & Spangler S. R., 1995, ApJ, 443, 209
Beck A.M., Lesch H., Dolag K., et al., 2012, MNRAS, 422, 2152
Beck A.M., Dolag K., Lesch H., Kronberg P.P., 2013, MNRAS, 435, 3575
Beck R., Brandenburg A., Moss D., Shukurov A., Sokoloff D., 1996, A&AR, 34, 155
Beck R., Wielebinski R., 2013, pss5.book, 641
Cordes J. M., & Lazio T. J. W. 2002, preprint (arXiv:astro-ph/0207156)
Dolag K., Grasso D., Springel V., Tkachev I., 2004, JETPL, 79, 583
Farrar G. R., Jansson R., Feain I. J., & Gaensler B. M., 2013, JCAP, 1, 23
Farrar G. R., 2014, C. R. Physique, 15, 339
Fauvet L., Macías-Pérez J. F., Aumont J., et al., 2011, A&A, 526, A145
Fauvet L., Macías-Pérez J.F., Désert F.X., 2012, APh, 36, 57
Fletcher A., Beck R., Shukurov A., Berkhuijsen E. M., Horellou C., 2011, MNRAS, 412, 2396
Giacinti G., Kachelrieß M., Semikoz D. V., Sigl G., 2011, APh, 35, 192
Górski K. M., Hivon E., Banday A. J., et al., 2005, ApJ, 622, 759
Harari D., Mollerach S., Roulet E., Sánchez F., 2002, JHEP, 3, 45
Haslam C.G.T., Klein U., Salter C.J., et al., 1981, A&A, 100, 209
Haslam C.G.T., Salter C.J., Stoffel H., Wilson W.E., 1982, A&AS, 47, 1
Haverkorn M., 2014, preprint (arXiv:1406.0283)
Heiles C., & Haverkorn M., 2012, SSRv, 166, 293
Jaffe T.R., Leahy J.P., Banday A.J., et al., 2010, MNRAS, 401, 1013
Jansson R., Farrar G.R., Waelkens A.H., Enßlin T.A., 2009, JCAP, 7, 21
Jansson R., Farrar G.R., 2012a, ApJ, 757, 14
Jansson R., Farrar G.R., 2012b, ApJL, 761, L11
Keivani A., Farrar G. R., Sutherland M., 2015, APh, 61, 47
Kitaura F. S., & Enßlin T. A. 2008, MNRAS, 389, 497
Letessier-Selvon A. for the Pierre Auger Collaboration, et al., 2013, preprint (arXiv:1310.4620)
Mao S.A., Gaensler B.M., Haverkorn M., et al., 2010, ApJ, 714, 1170
Mao S.A., McClure-Griffiths N.M., Gaensler B.M., et al., 2012, ApJ, 755, 21
Martel H., 2005, preprint (arXiv:astro-ph/0506540)
Miville-Deschênes M.-A., Ysard N., Lavabre A., et al., 2008, A&A, 490, 1093
Noutsos A., 2012, SSRv, 166, 307
Oppermann N., Junklewitz H., Robbers G., et al., 2012, A&A, 542, A93
Oppermann N., Junklewitz H., Greiner M., et al., 2014, preprint (arXiv:1404.3701)
Orlando E., Strong A., 2013, MNRAS, 436, 2127
Planck Collaboration, 2014a, preprint (arXiv:1405.0871)
Planck Collaboration, 2014b, preprint (arXiv:1405.0872)
Planck Collaboration, 2014c, preprint (arXiv:1405.0873)
Planck Collaboration, 2014d, preprint (arXiv:1405.0874)
Planck Collaboration, 2014e, preprint (arXiv:1406.7482)
Pshirkov M.S., Tinyakov P.G., Kronberg P.P., Newton-McGee K.J., 2011, ApJ, 738, 192
Schnitzeler D. H. F. M., 2010, MNRAS, 409, L99
Strong A. W., Moskalenko I. V., Ptuskin V. S., 2007, ARNPS, 57, 285
Strong A. W., Orlando E., Jaffe T. R., 2011, A&A, 534, A54
Strong A. W., Porter T. A., Digel S. W., Jóhannesson G., Martin P., Moskalenko I. V., Murphy E. J., Orlando E., 2010, ApJ, 722, L58
Sun X.-H., Reich W., Waelkens A., Enßlin T.A., 2008, A&A, 477, 573
Sun X. H., & Reich W., 2009, A&A, 507, 1087
Waelkens A., Jaffe T., Reinecke M., Kitaura F.S., Enßlin T.A., 2009, A&A, 495, 697
Widrow L.M., 2002, RvMP, 74, 775

This paper has been typeset from a TEX/ LATEX file prepared by the author.